PLASMA AND GAS PHASE KINETICS OF HIGH DENSITY SF_6 DISCHARGES

by

C. Lee, D. W. Hess, and M. A. Lieberman

Memorandum No. UCB/ERL M92/95

1 September 1992

PLASMA AND GAS PHASE KINETICS OF HIGH DENSITY SF_6 DISCHARGES

by

C. Lee, D. W. Hess, and M. A. Lieberman

Memorandum No. UCB/ERL M92/95

1 September 1992

ELECTRONICS RESEARCH LABORATORY

College of Engineering
University of California, Berkeley
94720

PLASMA AND GAS PHASE KINETICS OF HIGH DENSITY SF_6 DISCHARGES

by

C. Lee, D. W. Hess, and M. A. Lieberman

Memorandum No. UCB/ERL M92/95

1 September 1992

ELECTRONICS RESEARCH LABORATORY

College of Engineering
University of California, Berkeley
94720

Plasma and Gas Phase Kinetics of High Density SF_6 Discharges

C. Lee (Department of Chemical Engineering)
D. W. Hess (Department of Chemical Engineering)[1]
M. A. Lieberman (Department of Electrical Engineering and Computer Sciences)

University of California
Berkeley, CA 94720
(510) 642-2483

Abstract

The plasma equilibrium and gas phase chemistry of high density SF_6 discharge used for tungsten etching were studied. A self-consistent model was developed to determine positive ion, negative ion and electron densities, free radical density, ion fluxes, and electron temperature as functions of gas pressure, microwave input power, and cylindrical source diameter and length. For an electron cyclotron resonance (ECR) discharge, the reduction in radial transport due to the confining magnetic field was also modeled. The model predicted that the plasma electronegativity increases with increasing pressure and decreasing power, that F^- density is much smaller than SF_5^-, and that the SF_5^+ positive ion density increases roughly linearly with power, relatively independent of gas pressure.

Langmuir probes and OES(optical emission spectroscopy)/actinometry were used to obtain ion density, electron temperature, and fluorine atom concentration in an ECR discharge for comparison to the model results. CVD tungsten etch rate measurements showed that at low pressure, etch rate is fluorine atom limited, whereas at high pressure, it is ion flux limited. Effects of oxygen addition were also studied. Contrary to observations made in conventional RIE systems, fluorine atom concentration decreases as oxygen is added.

[1]currently at Lehigh University, Bethlehem, Pa

I. INTRODUCTION

As feature sizes of microelectronic devices decrease, processes and equipment requirements become more critical to microelectronics manufacturing. While high density plasma sources such as the ECR (electron cyclotron resonance), helical resonator, TCP (transformer-coupled plasma), and helicon are under extensive study, the focus is more on the plasma physics than the etch chemistry. However, etch kinetics and chemistry are important for better process control and more efficient approaches to process design.

In this report, we describe a self-consistent plasma equilibrium and gas phase chemistry model of SF_6, a widely used etchant gas for refractory metals. The initial reactor geometry and configuration used in this model is that of an electron cyclotron resonance discharge. However, the model is applicable to other high density source configurations including the TCP, helicon, etc. A self-consistent plasma and chemical kinetic model was developed to determine the electronegativity, species densities, and electron temperature as functions of input power, pressure, and source geometry. To determine the applicability of the model, experimental data were compared to the model results.

II. MODEL DEVELOPMENT

The purpose of the model was to establish a correlation between the plasma physics, the chemistry and the etch process. Gas phase kinetics, through electron-neutral collisions, generates ions and free radicals that are responsible for etching. Development of a physical-chemical model will establish relationships between microscopic discharge variables, i.e., ion density, electron temperature, F atom concentration, and macroscopic output and input variables, i.e., etch rate, power, and pressure.

A. Free-Fall and Diffusion Model

Assumptions used in the model were as follows:

1. Neutral species kinetics were excluded since only electronegativity and ion density were of concern in the initial development of the model.
2. Loss of positive ions to the pump was neglected; an order of magnitude calculation showed that this contribution is small compared to other loss mechanisms, such as ion/ion recombination and wall losses.

3. The model only has homogeneous gas phase reactions; surface reactions, such as fluorine passivation of chamber walls and adsorption/desorption of the etch surface, were not included.

4. SF_5^+ was the only positive ion considered initially; SF_3^+ was later added. These limitations are not fundamental and will be relaxed in future development of the model.

The model included ionic species only since our major concern was the amount of negative ions in the plasma and how ion density behaves with variations in microwave input power and pressure. Electron-neutral collision reactions considered were dissociative ionization, dissociative attachment, and ion/ion recombination.[9]

(I) $e + SF_6 \xrightarrow{k_1} SF_5^+ + F + 2e$ Dissociative Ionization

(II) $e + SF_6 \xrightarrow{k_3} SF_5^- + F$ Dissociative Attachment

(III) $e + SF_6 \xrightarrow{k_4} SF_5 + F^-$ Dissociative Attachment

(IV) $SF_5^+ + SF_5^- \xrightarrow{k_5} 2SF_5$ Ion/ion recombination

(V) $SF_5^+ + F^- \xrightarrow{k_6} SF_6$ Ion/ion recombination

Because of its strong dependence on electron temperature, the rate constant of the dissociative ionization reaction was calculated by integrating the electron-neutral cross section[18] of the reaction over an assumed Maxwellian electron energy distribution in velocity space, i.e.,

$$k_i = \langle \sigma v \rangle_i = 4\pi \int_0^\infty f(v)\, \sigma(v)\, v^3 dv$$

The collision cross sections for dissociative attachment and ion/ion recombination are weak functions of electron temperature; therefore, an average value was calculated over the temperature range of 1 to 7 Ev.[15,16] Rate constants used in reactions (I) - (V) are as follows:

$k_1 = 9.21 \times 10^{-8} \exp(-15.2/kTe)\ cm^3/s$

$k_3 = 7.34 \times 10^{-10}\ cm^3/s$

$k_4 = 3.3 \times 10^{-12}\ cm^3/s$

$k_5 = 1 \times 10^{-7}\ cm^3/s$

$k_6 = 1 \times 10^{-7}\ cm^3/s$

From the reactions, one can write steady state rate equations for the species SF_5^+, SF_5^-, and F^-. Two types of loss mechanisms for positive ions were separately considered: free-fall and diffusion. Free-fall loss, which is the simplest case of ion loss to the wall, occurs when ions are generated through electron-neutral collisions and "free-fall" to the chamber walls without suffering significant collisions with other species in the plasma. This loss mechanism, however, is not sufficient to describe what happens in a high density plasma source at reasonable pressures, such as an ECR, especially in the presence of a magnetic field. Hence, free-fall losses must be replaced by diffusional losses. For an ECR system in a cylindrical geometry, diffusional losses occur in both radial and axial directions (with respect to the magnetic field). In the diffusional loss mechanism, ions are lost to the sidewalls by colliding with other species; for radial (cross field) diffusion, upon collision, ions "hop" from one field line to the other in a random-walk process until they arrive at the wall surface and are lost.[1] Because the dominating mechanism here is collisional, radial diffusion is enhanced at higher pressures where the collision frequency between ions and neutrals are greater. Axial diffusion, on the other hand, is inversely proportional to the ion-neutral collision frequency, which is proportional to pressure. Therefore, the diffusional losses in the axial direction decrease with increasing pressure.

Energy and particle conservation equations were used to obtain species concentrations and electron temperature. Particle conservation equations were written from steady state rate equations for the positive ionic species involved,

(1) $$k_1 n_e n_{SF6} - k_5 n_{SF5^-} n_{SF5+} - k_6 n_{F^-} n_{SF5+} - U_B n_{SF5+}/L = 0$$

The last term in equation (1), where $U_B = (kT_e/M)^{1/2}$ is the ion Bohm velocity, and L is the discharge length, represents the free-fall loss mechanism for positive ions. In an electron cyclotron resonance discharge, the loss mechanisms are more complicated, especially in the presence of a magnetic field.[1] For the diffusion

loss mechanism, the last term in equations (1) is replaced by a term that accounts for losses from axial and radial diffusion.

$$\frac{U_B}{L} \rightarrow \frac{D_\parallel}{\Lambda_\parallel^2} + \frac{D_\perp}{\Lambda_\perp^2}$$

where $D_\parallel$ = axial diffusion coefficient, cm^2/s

$= kT_i/M\nu$

$D_\perp$ = radial diffusion coefficient, cm^2/s

$= D_\parallel/(1 + \omega_c^2 \tau^2)$

$\Lambda_\parallel$ = effective axial diffusion length[17], cm

$= L/\pi$

$\Lambda_\perp$ = effective radial diffusion length[17], cm

$= R/2.405$

with T_i = ion temperature

M = ion mass

ν = ion-neutral collision frequency[13]

τ = $1/\nu$

ω_c = cyclotron frequency = eB/M

B = magnetic field

L = length of cylindrical reactor

R = radius of reactor

The equation given by $D_\parallel$ is the free-diffusion coefficient. Because of the large mass difference between electrons and ions, electrons move much faster than ions, and an electric field is set up which accelerates ions and retards electrons. Therefore, $D_\parallel$ must be modified to take into account the effects of the electric field, i.e., $D_\parallel$ replaced with $D_{a,\parallel}$, which is the ambipolar diffusion coefficient.[1] The E field effect is found by setting $r_i = r_e = r$, since fluxes of oppositely charged species must be equal. The flux can be

written as

$$r_j = Z_j \mu_j n_j E - D_j \nabla n_j,$$

where μ_j = mobility of the jth species,

Z_j = charge associated with species j,

D_j = free diffusion coefficient of species j,

and n_j = density of species j.

With the presence of negative ions, equating positive and negative species fluxes gives

$$r_+ = r_e + r_- .$$

Substitution of appropriate terms gives

$$\mu_+ n_+ E - D_+ \nabla n_+ = -\mu_e n_e E - D_e \nabla n_e - \mu_- n_- E - D_- \nabla n_- .$$

After obtaining the electric field as functions of mobility, species density, and diffusion coefficient,

$$E = f(\mu_j, D_j, n_j, \nabla n_j),$$

the expression for E can be substituted back into the flux equation to determine the ambipolar diffusion coefficient,[19]

$$D_{a,+} = D_+ - EZ_+\mu_+ / \nabla n_j/n_j \ ,$$

where $D_{a,+} = D_{a,-}$.

The steady state equations for negative ion species, SF_5^- and F^-, are

(2) $$k_3 n_e n_{SF6} - k_5 n_{SF5^-} n_{SF5+} = 0$$

(3) $$k_4 n_e n_{SF6} - k_6 n_{F^-} n_{SF5+} = 0$$

where k_i = rate constant of the ith reaction, cm^3/s,

n_j = density of the jth species, molecules(atoms)/cm^3.

Since the bulk of the plasma is essentially neutral, an additional equation can be written,

(4) $$n_{SF5+} = n_e + n_{F^-} + n_{SF5^-}$$

The power balance equation assumes all the microwave input power is absorbed by the plasma; energy is lost through ion flux to the chamber walls and the generation of ion-electron pairs.

$$(5) \qquad P_f = n_{SF_5^+} U_B e \varepsilon_T$$

where $\varepsilon_T = \varepsilon_L + \varepsilon_i + \varepsilon_e$?, 12

ε_L = collisional electron energy loss per ion lost to the wall

ε_i = energy of an ion striking endwall ≈ 5 - 8 T_e

ε_e = energy of an electron striking the endwall ≈ 2 T_e

P_f = microwave input power (W/cm^2)

e = electron charge, 1.6×10^{-19} C

U_B = Bohm velocity = $(kT_e/M)^{1/2}$ cm/s

Equations (1) - (5) are solved numerically to obtain n_{SF5+}, n_{SF5^-}, n_{F^-}, n_e, and T_e as functions of input power and pressure.

B. Generation of SF_3^+ versus SF_5^+

For gases with complicated molecular structures such as SF_6, there are many possible reactions that generate positive ions. One important reaction is the generation of SF_3^+ through a multiple step process of dissociation and dissociative ionization, to a concentration that is comparable or greater than the concentration of SF_5^+. The dissociation reaction generates SF_4 and two fluorine atoms from SF_6,

(VI) $e + SF_6 \xrightarrow{k_7} SF_4 + 2F + e$ $\qquad k_7 = 8.0 \times 10^{-8}\, e^{-10/kTe}\ cm^3/s.$

The neutral and stable SF_4 molecules then undergo dissociative ionization to generate SF_3^+,

(VII) $e + SF_4 \xrightarrow{k_8} SF_3^+ + F + 2e$ $\qquad k_8 = 9.21 \times 10^{-8}\, e^{-12.4/Kte}\ cm^3/s$

Another possible mechanism for generating SF_3^+ is direct electron impact dissociative ionization of SF_6, where three fluorine atoms are formed along with the SF_3^+ ion,

(VIII) $e + SF_6 \longrightarrow SF_3^+ + 3F + 2e$

This mechanism, however, has a much smaller contribution than the multistep process.[6] Therefore, it was not included in the analysis; only reactions (I), (VI), and (VII) were used.

Steady state rate equations were written ,

(6) $k_7 n_e n_{SF6} - k_8 n_e n_{SF4} - k_r n_{SF4} = 0$

(7) $k_1 n_e n_{SF6} - U_{B,SF5+} n_{SF5+}/L = 0$

(8) $k_8 n_e n_{SF4} - U_{B,SF3+} n_{SF3+}/L = 0$

The last term in equation (6) is the pumping loss of neutral SF_4, with $k_r = 0.125/s$, which is the inverse of the residence time. Equations (6) - (8) were solved to obtain the ratio of SF_{3+}/SF_{5+},

$$\frac{n_{SF_3^+}}{n_{SF_5^+}} = \frac{k_7 k_8 U_{B,SF_5^+}}{k_1 U_{B,SF_3^+}} \frac{n_e}{k_8 n_e + k_r} \quad .$$

When the electron density is low, i.e., $k_8 n_e << k_r$, the equation becomes

$$\frac{n_{SF_3^+}}{n_{SF_5^+}} = \frac{k_7 k_8 U_{B,SF_5^+}}{k_1 U_{B,SF_3^+}} \frac{n_e}{k_r} \quad ,$$

whereas at high electron densities, i.e., $k_8 n_e >> k_r$, we have

$$\frac{n_{SF_3^+}}{n_{SF_5^+}} = \frac{k_7 U_{B,SF_5^+}}{k_1 U_{B,SF_3^+}} \quad .$$

The ratio of the Bohm velocities, $U_{B,SF5+}/U_{B,SF3+}$ is an inverse ratio of the ion masses.

III. EXPERIMENT

The ECR system used here has been described elsewhere.[14] The reactor configuration is shown in Figure 1. Patterned tungsten samples were supplied by Motorola; the sample structure and procedures for the experiment were described in a previous report.[11] Optical emission spectroscopy (OES) using argon as the actinometry gas was used to obtain fluorine atom concentration. No wafer samples were in the chamber when OES data were taken; the plasma scan system was located downstream at the waferholder position. (see Figure 1) A Langmuir probe was used to obtain ion density.

A Plasma Therm Scan system was used for optical emission spectroscopy. This is an in-situ, real time analytical method to monitor concentrations of plasma species.[5,2] Concentrations of active species are directly

proportional to the intensity of their optical emission lines at a specific wavelength. In principle, this optical property allows one to readily obtain the concentration of atomic species in a plasma. A tracer gas is needed, however, since the translation from intensity to concentration requires a knowledge of the collision cross section of the species and the electron energy distribution function of the plasma, which are not readily available in most cases. The tracer, normally an inert gas with similar collision cross section as the atomic species of interest, provides a relative concentration for the atomic species under different plasma conditions. The wavelength scanner was programmed with a scan range of 690 to 790 nm. This specific range was chosen because the emission line for the excited fluorine species is 703.7 nm, and that of argon is at 750.4 nm.

Relative fluorine atom concentrations are obtained for variations in power and pressure; the effect of oxygen addition was also studied. Argon gas with a pressure of 0.05 mTorr was added via a needle valve. The total flowrate into the system was maintained at 3.0 SCCM. For power and pressure variations, only SF_6 was used, with microwave input power from 300 - 700 Watts, and pressure from 0.4 to 5.0 mTorr. Effects of oxygen on fluorine atom concentration were investigated by obtaining optical spectra for 0 - 50 percent O_2 added.

IV. RESULTS AND DISCUSSIONS

A. Kinetic Model

Results of the free-fall and the diffusion models are shown in Figures 2 - 6. Parameters used in the model are

$L = 40$ cm,

$R = 7.6$ cm,

$T_+ = T_- = 0.5$ eV,

$\varepsilon_T = 400$ eV,

$B = 1000$ Gauss.

Figure 2 shows that the positive ion density increases linearly with increasing microwave power; this trend is also observed experimentally, as seen in Figure 6a. The pressure variation, on the other hand, had little effect on the positive ion density in both the free-fall and diffusion models; this does not agree with

experimental data (Figure 6b). The source of the discrepancy is in the spatial variation of the ions in the system. The model assumed a uniform ion density within the source chamber. As ions are generated and diffuse downstream, a significant number are lost to the sidewalls; as a result, the density downstream will be much less than that within the source. A first order approximation to this diffusive behavior is a decreasing exponential dependence, $n_i \approx e^{-bz}$, where b is proportional to pressure, and z is the axial position; a detail solution showing this behavior is presented by Stewart et al.[21] Since the experimental data was taken downstream, the value from the model must be scaled with the exponential decrease before a comparison can be made.

Figure 3 shows the concentration of negatively charged species in the plasma under different process conditions, with power varying from 0.3 to 10 W/cm^2, and pressure from 0.1 to 100 mTorr. The ratio of n_e/n_{SF5+} is a measure of the number of negative ions. For a positive-ion dominated plasma, $n_e \approx n_{SF5+}$, ($n_e/n_{SF5+} \approx 1$), whereas for the negative-ion dominated case, $n_e << n_{SF5+}$, ($n_e/n_{SF5+} << 1$). If a large number of negative ions are present, quasineutrality requires a low n_e. From Figure 3, one can see that the concentration of negative ions decreases with increasing power and decreasing pressure. Hence high density, low pressure sources are more electropositive than typical RIE systems.

The variation of electron temperature with power and pressure is shown in Figure 4. The free-fall model predicts that the electron temperature is higher at lower input power, which is contrary to the behavior of an electropositive plasma, where electron temperature does not depend on power.[7, 12] Keeping in mind that electron temperature is an average value obtained from the electron energy distribution function, this observation is consistent with the electronegative behavior of the plasma at low powers: the low energy electrons shifts the electron temperature to a higher value to sustain the ionization required. The diffusion model, on the other hand, shows a much weaker dependence of T_e on power and shows better agreement with experimental data (Figure 7a). Both models show that electron temperature decreases with increasing pressure, as measured by the Langmuir probe (Figure 7b). The decrease is attributed to the decrease in the ionization rate constant for particle balance at higher pressures.

The dependence of SF_5^- on power and pressure is shown in Figure 5. At high pressure, n_{SF5^-}

increases nearly linearly with increasing power, whereas at low pressures, n_{SF5^-} increases initially, and then levels off asymptotically as power increases. The pressure dependence can be explained through the electron temperature. As pressure increases, electron temperature decreases, making available more lower energy electrons for attachment; the negative ion density increases as a result. The dependence of negative ion density on power is not as obvious. As power increases, more energy is added to the plasma, increasing the concentration of SF_5 and F atoms/molecules through dissociation, which are readily available for attachment. At lower pressure, 0.1 and 0.5 mTorr, electron temperature is higher, providing a limited number of low energy electrons, and the negative ion density levels off. At high pressures, negative ion density increases linearly with power since the electron temperature is lower, making available a large number of low energy electrons for attachment. There are no essentially no differences between the free-fall and diffusion model for negative ion density, since the loss mechanisms applied to positive ions only. The only loss mechanism for negative ions is ion/ion recombination.

The behavior of F^- with power and pressure is the same as that of SF_5^-; the density of F^- is much smaller, however. The ratio of n_{SF5^-}/n_{F^-} is independent of power and pressure with a value of approximately 200.

B. Generation of SF_3^+ versus SF_5^+

Figure 8 shows the ratio of SF_{3+}/SF_{5+} versus electron density. For low density cases, i.e., n_e between 10^7 - 10^8 cm^{-3}, SF_{5+} was the dominant ion. As electron densities increase, the ratio also increases, rising linearly through a transition region. At electron densities greater than 10^{10} cm^{-3}, the ratio remains constant, in which case SF_{3+} was the dominant ion. The reader should keep in mind that this is a simple model that included only three reactions (see Section IIB); the results should be viewed as providing only qualitative behavior.

The electron temperature of the system also affects the ratio of SF_{3+}/SF_{5+}. As shown in Figure 8, the ratio increases with decreasing electron temperature, which suggested the multistep process of generating SF_{3+} is more likely when the electron temperature is lower. This observation agrees well with the lower threshold energy for dissociation and dissociative ionization of SF_6 and SF_4, respectively.

C. Diagnostics

Ion density and fluorine atom concentration were measured using Langmuir probe and optical emission spectroscopy/actinometry. The qualitative behavior of these plasma parameters along with etch rate information, was obtained for different process environments.

Figure 9 shows a typical optical emission spectrum with scan range from 690 to 790 nm. Changes in the F^* (703.7 nm) and the Ar^* (750.4 nm) peaks were monitored for dependence on power, pressure, flowrate, and oxygen addition. Figure 10 shows the behavior of ion density, relative fluorine atom concentration, and etch rate with oxygen addition. Data were taken at constant microwave power of 500 W and pressure of 1 mTorr; for etch rate data, the waferholder was RF biased to give a DC voltage of - 60 V. Neither ion density nor etch rate was affected when oxygen was added into the system. The fluorine atom concentration, however, decreased with oxygen addition. This observation is contrary to what is observed in parallel plate systems.[7,3] In an RIE reactor, fluorine concentration is enhanced by the addition of oxygen, peaking at approximately 10-15% addition, depending upon the reactor configuration and operating condition. This behavior may be due to differences in operating pressure; the total pressure in an RIE system is typically two orders of magnitude greater than the pressure in an ECR. Under such circumstances, the gas phase reactions responsible for generating fluorine atoms might be overshadowed by surface effects, where fluorine passivation of the chamber wall and wafer surface adsorption are dominating.

There are at least two possible mechanisms that control the etch rate: ion-enhanced and chemical reactions. It has been proposed that the etching of tungsten involves the formation of WF_6, a volatile product that is readily desorbed from the tungsten surface once it has been formed.[4] Energetic ions bombarding the surface will also help enhanced the etch rate. This mechanism, however, is much more complicated and is currently under extensive study. The purpose of our study is to determine whether the etch rate is controlled by a single or multiple mechanisms. From Langmuir probe studies (Figures 6a and b), we observed that the ion density peaks at approximately 0.5 mTorr; and decreases exponentially as pressure increases. Therefore, to create a condition where the etch rate is limited by fluorine atom concentration and the ion density is in abundance, we must operate in the low pressure regime. On the other hand, operating at high pressures will

provide excess fluorine, with low ion density, providing the case where the ion flux is the limiting factor.

Figure 11 shows the dependence of ion density, fluorine atom concentration, and etch rate on SF_6 flowrate. With the pumping speed remaining constant, increasing the flowrate into the system will cause the pressure to rise due to changes in residence time, thus yielding the desired operating conditions. Ion density, measured by a Langmuir probe, is a maximum at a pressure of 0.4 mTorr, and decreases as the pressure is increased. The relative fluorine concentration is obtained through OES/actinometry, as described in Section III. As the pressure increases, fluorine concentration also increases, providing the excess fluorine and limited ion flux condition. Tungsten etch rates obtained under the same operating conditions are also shown in Figure 11. At low pressures, etch rate is fluorine atom limited, whereas for high pressures, it is ion flux limited. A mechanism similar to this was observed by Joubert et al.,[8] for the etching of photoresist by oxygen, where

$$\frac{1}{ER} \propto \frac{1}{n_i} + \frac{1}{n_a}$$

with ER is the etch rate, and n_i and n_a are the ion density and atomic species concentration, respectively.

D. Future Work

The kinetic model will be modified to include the self-consistent generation of SF_3^+ ions, since for a high density source such as the ECR, SF_3^+ appears to be the dominating positive species. In addition, neutral fluorine chemistry will be incorporated into the model. Results from the free radical chemistry can be compared to the experimental data, and move us one step closer to having a more complete model in describing the etch mechanism in high density plasma sources. Further experiments will be performed to separate the effects of flowrate and residence time on ion density, F atom concentration, and etch rate. The model will also be applied to different high density sources such as an inductively coupled system. The only modification is the inclusion/exclusion of the magnetic field and changes in the source geometry.

V. CONCLUSIONS

An analytical model was established for the kinetics of an SF_6 plasma in a high density source. Electron temperature, electron density, and positive and negative ion density were solved self-consistently as

functions of reactor geometry, microwave input power, and pressure. The results showed that the negative ion concentration increases with increasing pressure and decreases with increasing power.

Mechanisms that controlled the etch rate were studied, namely, ion-enhanced etch and chemical etch. Ion density, fluorine atom concentration, and etch rate were obtained under identical process conditions to minimize unnecessary variations. We have found that at low pressures, the etch rate was fluorine-limited, whereas for high pressures, the etch rate was ion-flux limited.

ACKNOWLEDGEMENTS

This work was supported by the Motorola Semiconductor Products Sector in Phoenix, AZ. The authors would like to thank J. Bukhman and D. Weston of Motorola for providing the multilayer tungsten structures, B. Lynch for assistance on plasma diagnostic techniques, and J. Benasso for helping to troubleshoot the equipment whenever necessary.

REFERENCES

1. Chen, F.F., *Introduction To Plasma Physics and Controlled Fusion*, Plenum Press, New York, pp.169-173, 1984.

2. d'Agostino, R., V. Colaprico, and F. Cramarossa, "The use of 'actinometer' gases in optical diagnostics of plasma etching mixtures: SF_6-O_2", *Plsm. Chem. Plsm. Proc.*, **1**, pp.365-375, 1981.

3. d'Agostino, R., and D. L. Flamm, "Plasma etching if Si and SiO_2 in SF_6-O_2 mixtures", *J. appl. Phys.*, **52**, pp. 162-167, 1981.

4. Durandet, A., Y. Arnal, J. Pelletier, and C. Pomot, "Anisotropy and kinetics of the etching of tungsten in SF_6 multipolar microwave plasma", *J. Appl. Phys.*, **67**, pp. 2298-2302, 1990.

5. Gottscho, R.A., and T. A. Miller, "Optical techniques in plasma diagnostics", *Pure & Appl. Chem.*, **56**, pp. 189-208, 1984.

6. Heller, S.R., and G.W.A. Milne, eds., *EPA/NIH Mass Spectral Data Base,* NSRDS-NBS, **63**, suppl. 1 (1980).

7. Hess, D.W., "Tungsten and tungsten silicide etching in halogenated Plasmas", *Solid State Tech.*, pp. 97-103, 1988.

8. Joubert, O., J. Pelletier, and Y. Arnal, "The etching of polymers in oxygen-based plasmas: a parametric study", *J. Appl. Phys.*, **65**, pp. 5096-5100, 1989.

9. Kline, L.E., "Electron and chemical kinetics in the low-pressure RF discharge etching of silicon in SF_6", *IEEE Trans. on Plsm. Sci.*, **PS-14**, pp. 145-155, 1986.

10. Kline, L.E., D. K. Davies, C. L. Chen, and P. J. Chantry, "Dielectric properties for SF_6 and SF_6 mixtures predicted from basic data", *J. Appl. Phys.*, **50**, pp. 6789-6798, 1979.

11. Lee, C., D. W. Hess, and M. A. Lieberman, "Plasma etching of CVD tungsten using ECR discharges", UCB/ERL Memorandum, M91/92, October 16, 1991.

12. Lieberman, M.A., EE239A lecture notes, University of California, Berkeley, Fall 1990.

13. Lyman, J.L., "Computer model of the SF_6-H_2 electrical discharge chemical laser", *Appl. Opt.*, **12**, pp.2736-2747, 1973.

14. Lynch, B., S. Das, M.A. Lieberman, and D.W. Hess, "Electron cyclotron resonance etching of silylated photoresist", UCB/ERL Memorandum, M92/25, March 5, 1992.

15. Nimura, T., and M. Hayashi, "Importance of attachment cross-sections of F^- formation for the effective ionization coefficients in SF_6 ", *J. Phys. D.*, **17**, pp. 2215-2223, 1984.

16. Novak, J.P., and M.F. Frechette, "Transport coefficients of SF_6 and SF_6-N_2 mixtures from revised data", *J. Appl. Phys.*, **55**, pp. 107-119, 1984.

17. Phelps, A.V., "The diffusion of charged particles in collisional plasmas: free and ambipolar diffusion at low and moderate pressures", *J. Res. Natl. Inst. Stand. Technol.*, **95**, pp. 407-431, 1990.

18. Rapp, D., and P. Englander-Golden, "Total cross sections for ionization and attachment in gases by electron impact. I. Positive ionization", *J. Chem. Phys.*, **43**, pp. 1464-1479, 1965.

19. Rogoff, G.L., "Ambipolar diffusion coefficients for discharges in attaching gases", *J. Phys. D: Appl. Phys.*, **18**, pp. 1533-1545, 1985.

20. Stanski, T., and B. Adamczyk, "Measurements of dissociative ionization cross sections of SF_6 by using double collector cycloidal mass spectrometer", *Int. J. Mass Spectrom. and Ion Phys.*, **46**, pp.31-34, 1983.

21. Stewart, R.A., B. Troyanovsky, and M.A. Lieberman, "Modeling magnetic bucket confinement in an ECR plasma processing reactor", *poster presentation at the IEEE conference on Plasma Science*, Williamsburg, VA 1991.

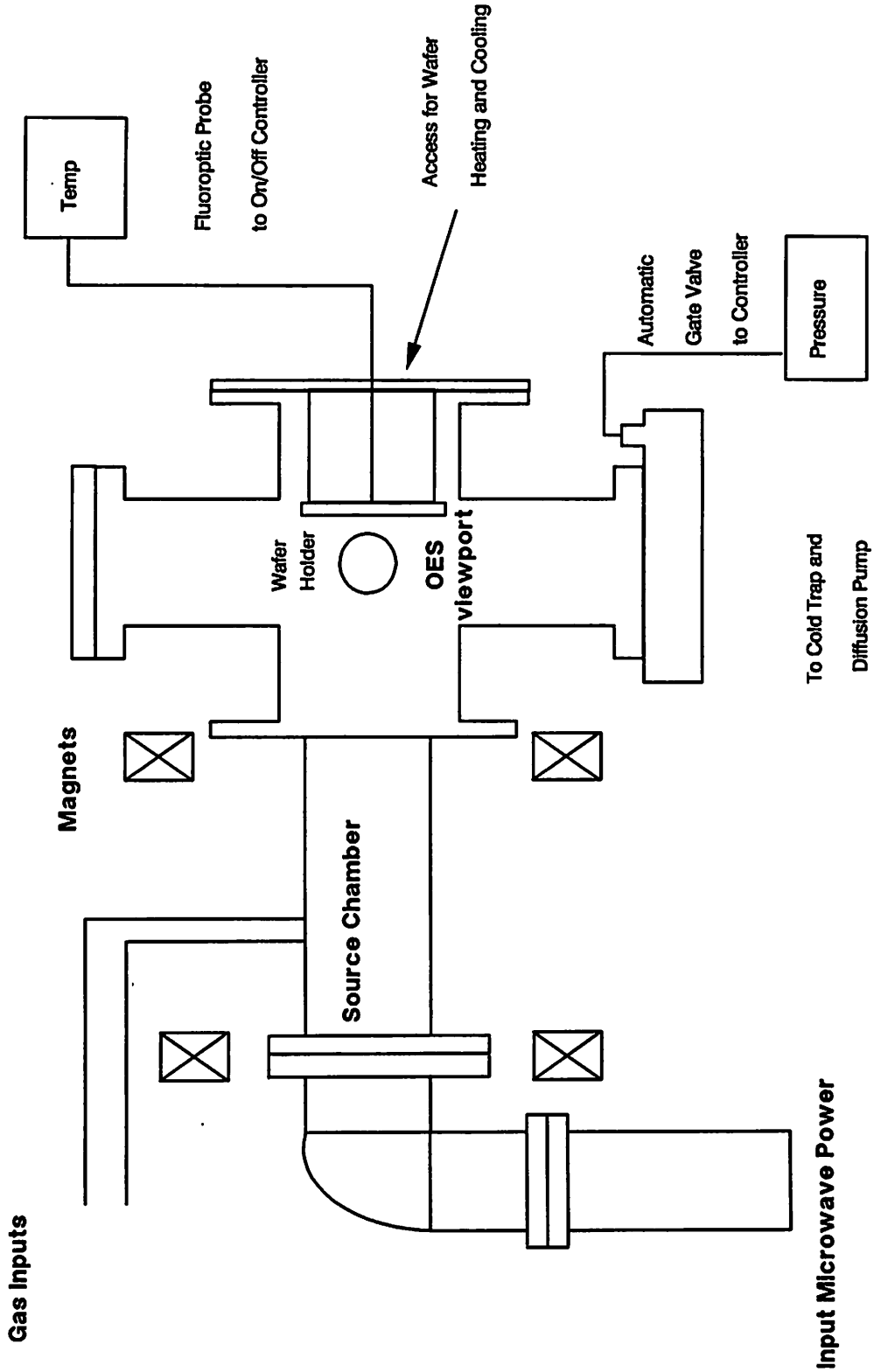

Figure 1. ECR system consisting of source and process chamber.

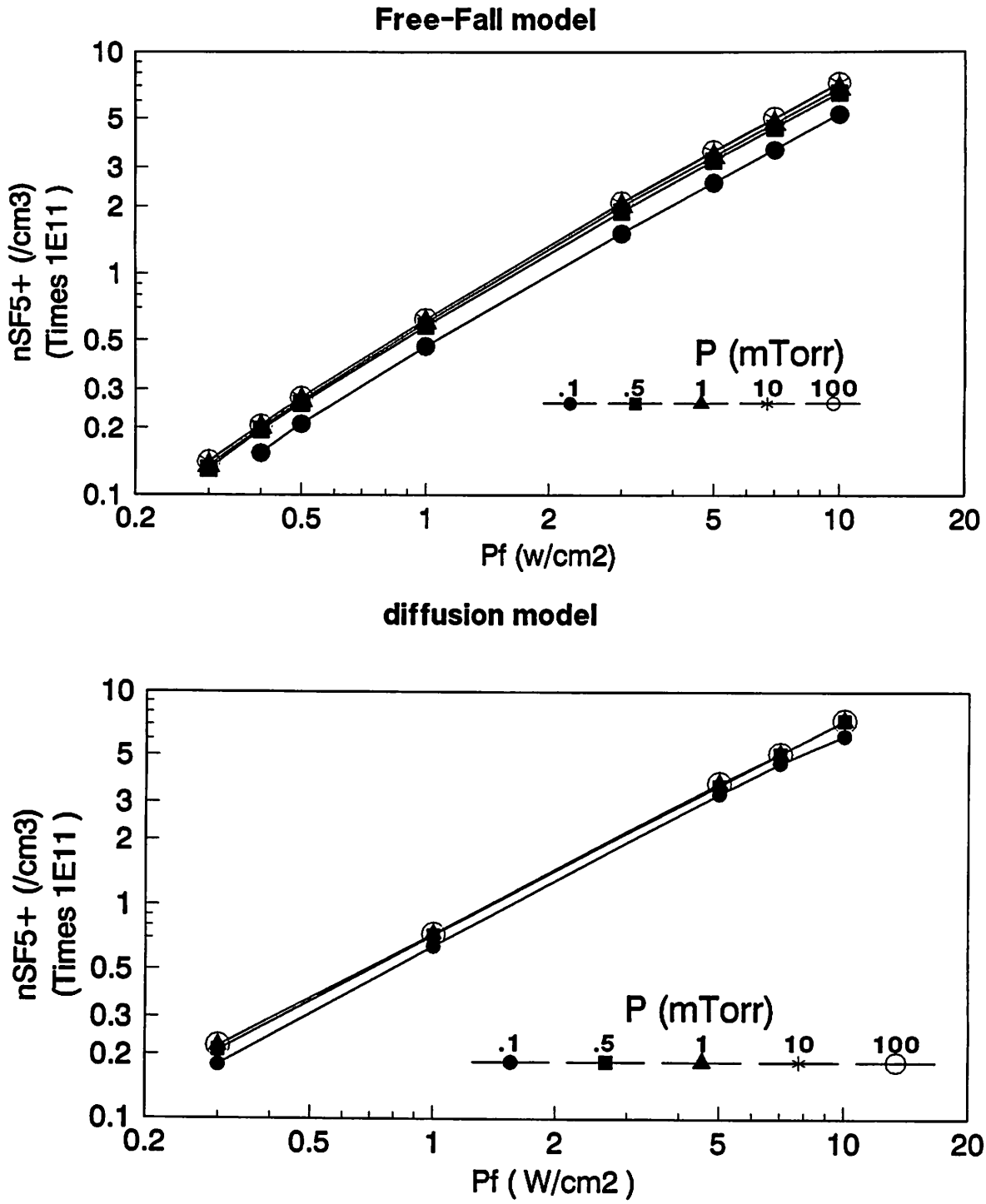

Figure 2. Positive ion density versus power and pressure.

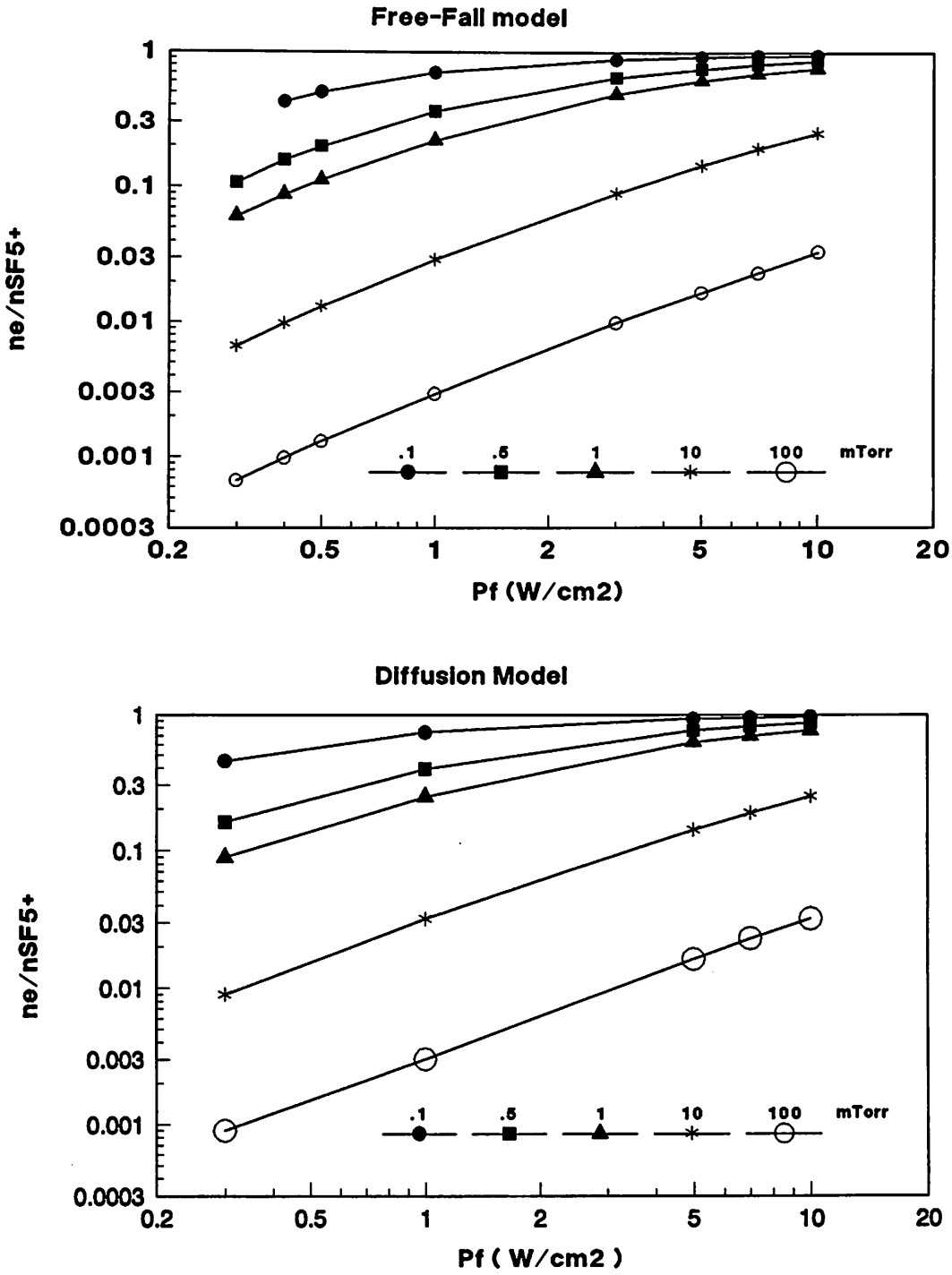

Figure 3. n_e/n_{SF5+} versus power and pressure.

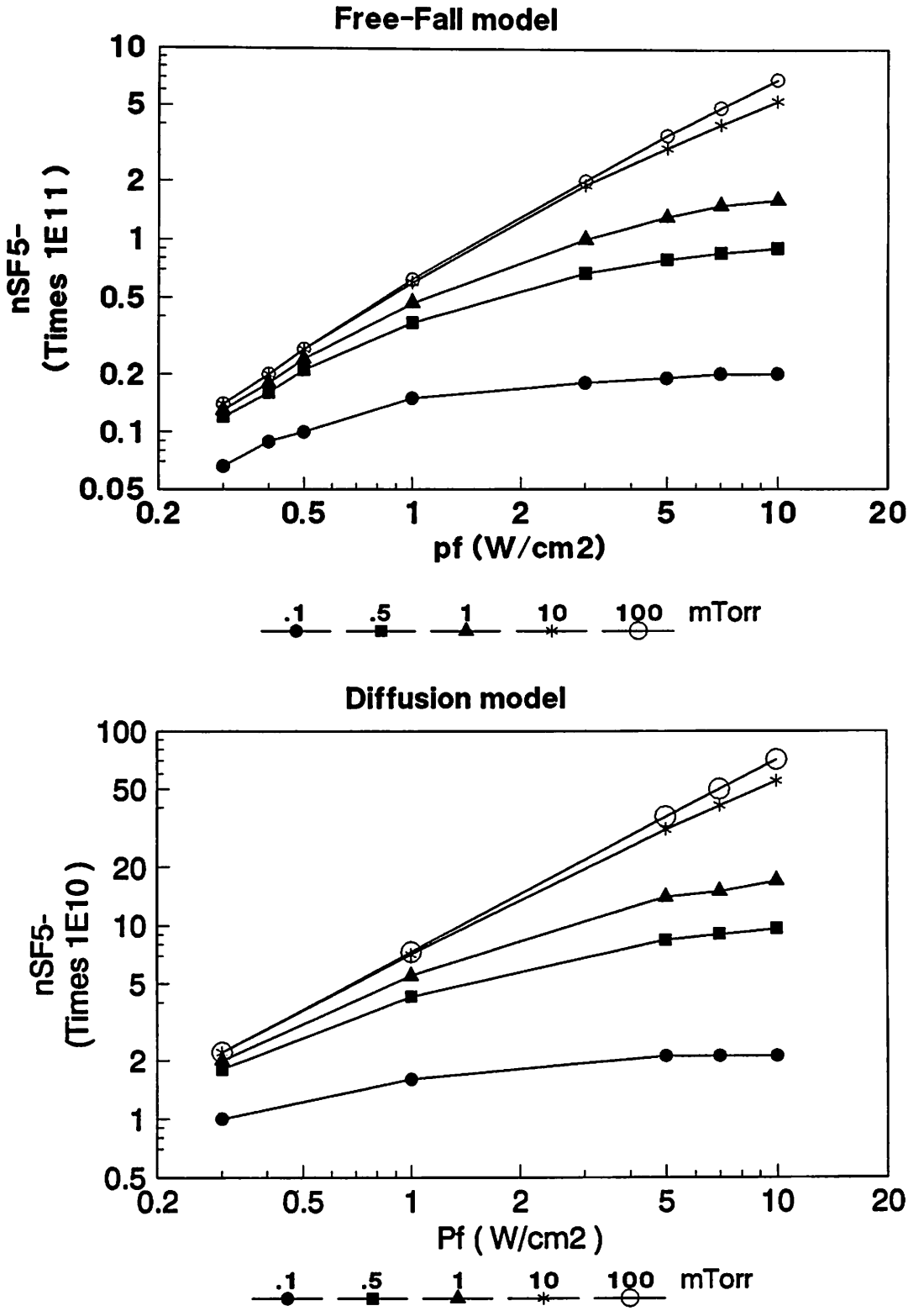

Figure 5. n_{SF5^-} versus power and pressure.

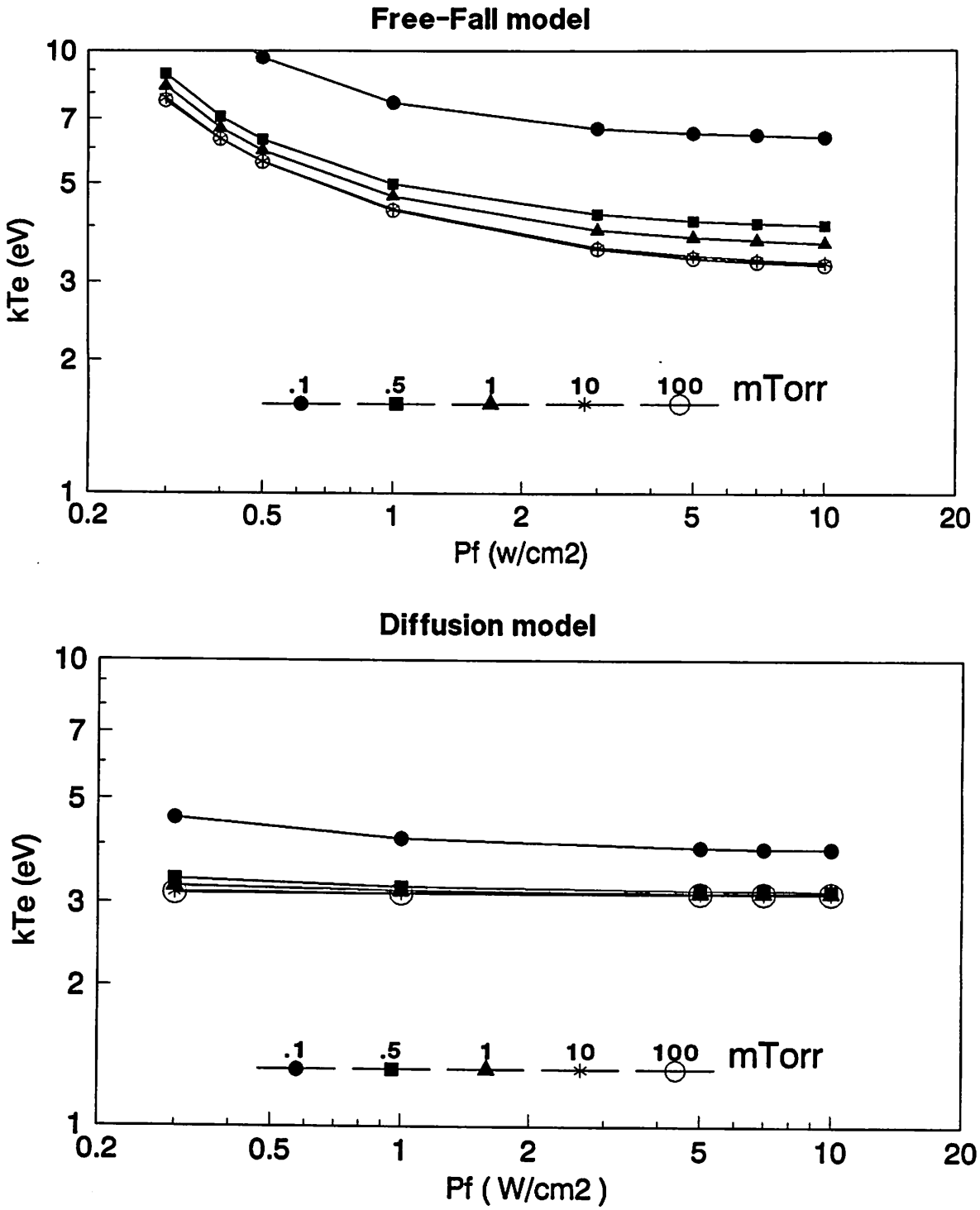

Figure 4. Electron temperature versus microwave power and pressure.

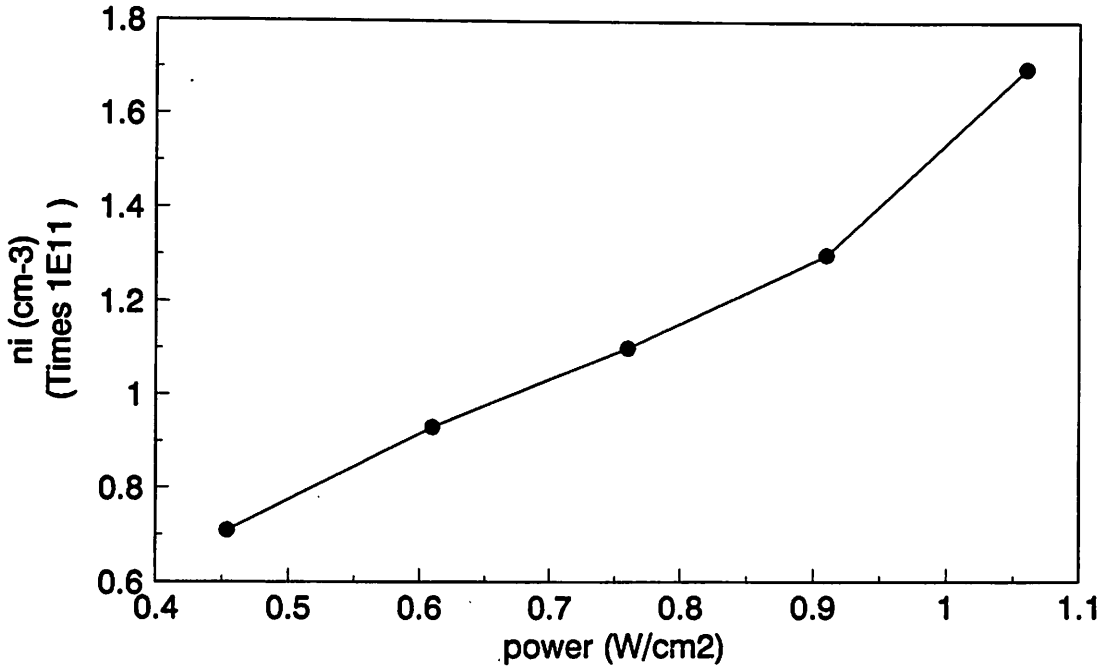

Figure 6a. Ion density versus microwave power in SF6 plasma.

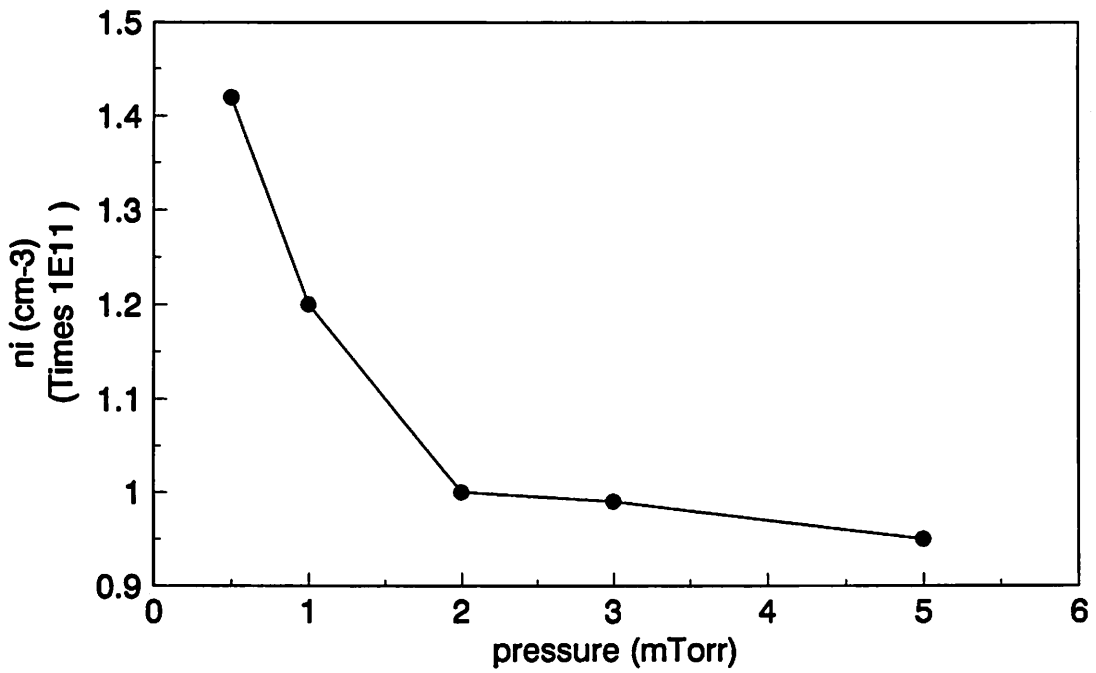

Figure 6b. Ion density versus pressure in SF6 plasma.

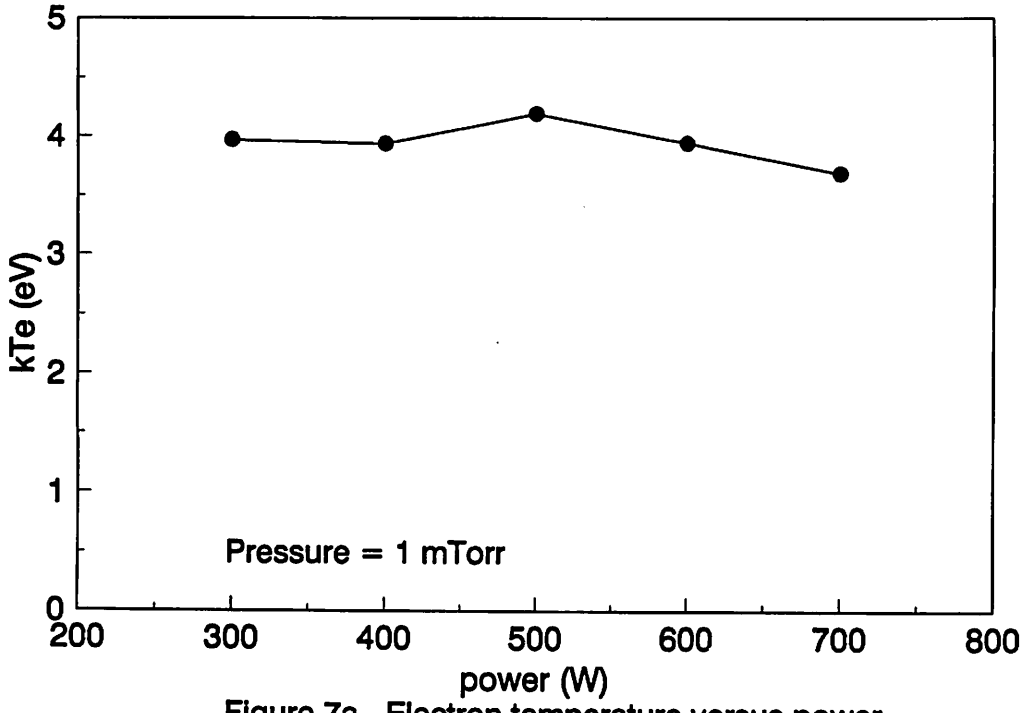

Figure 7a. Electron temperature versus power.

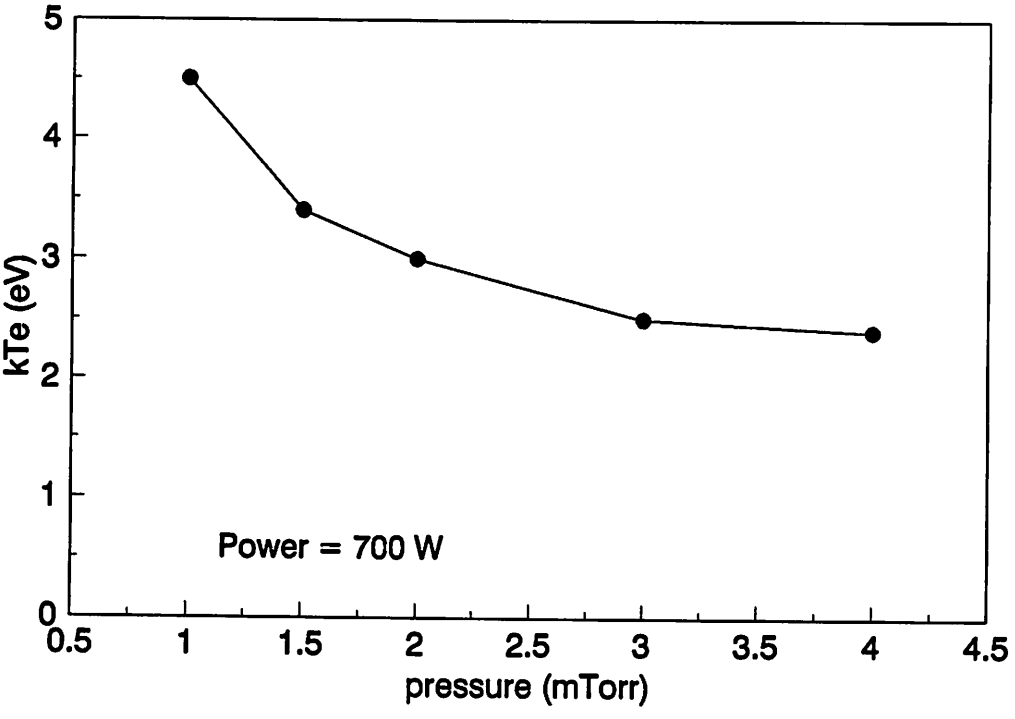

Figure 7b. Electron temperature versus pressure.

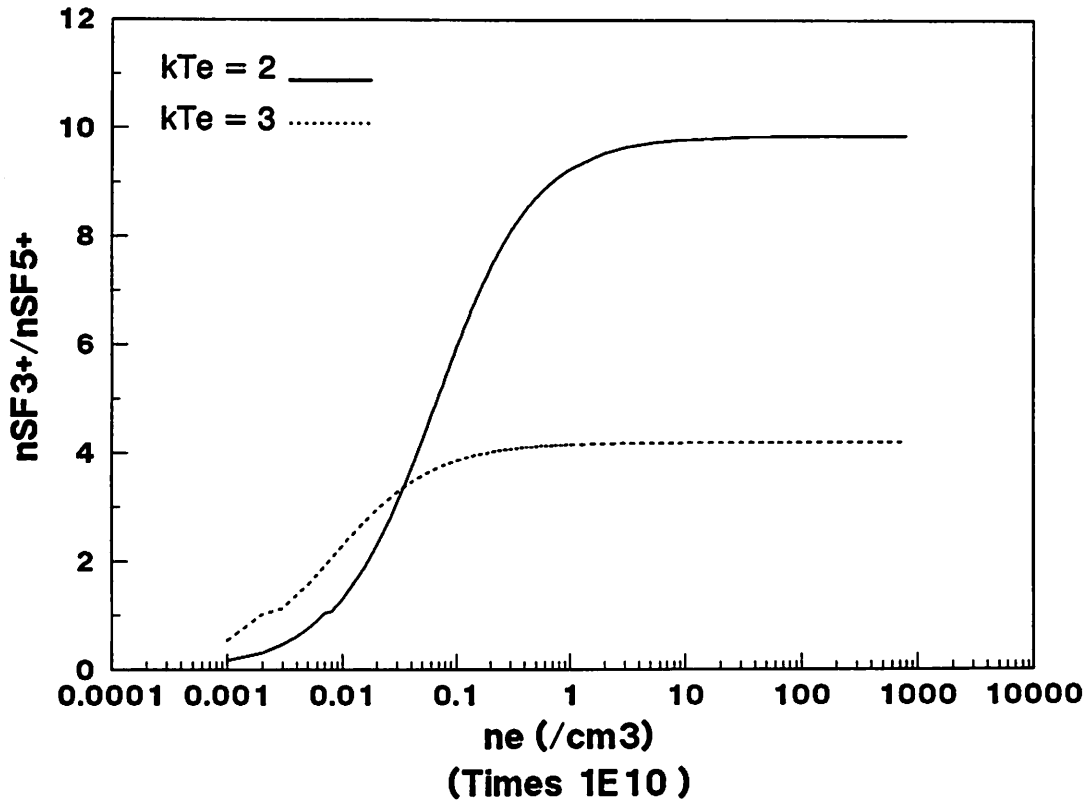

Figure 8. Ratio of n_{SF3+}/n_{SF5+} versus electron density and electron temperature.

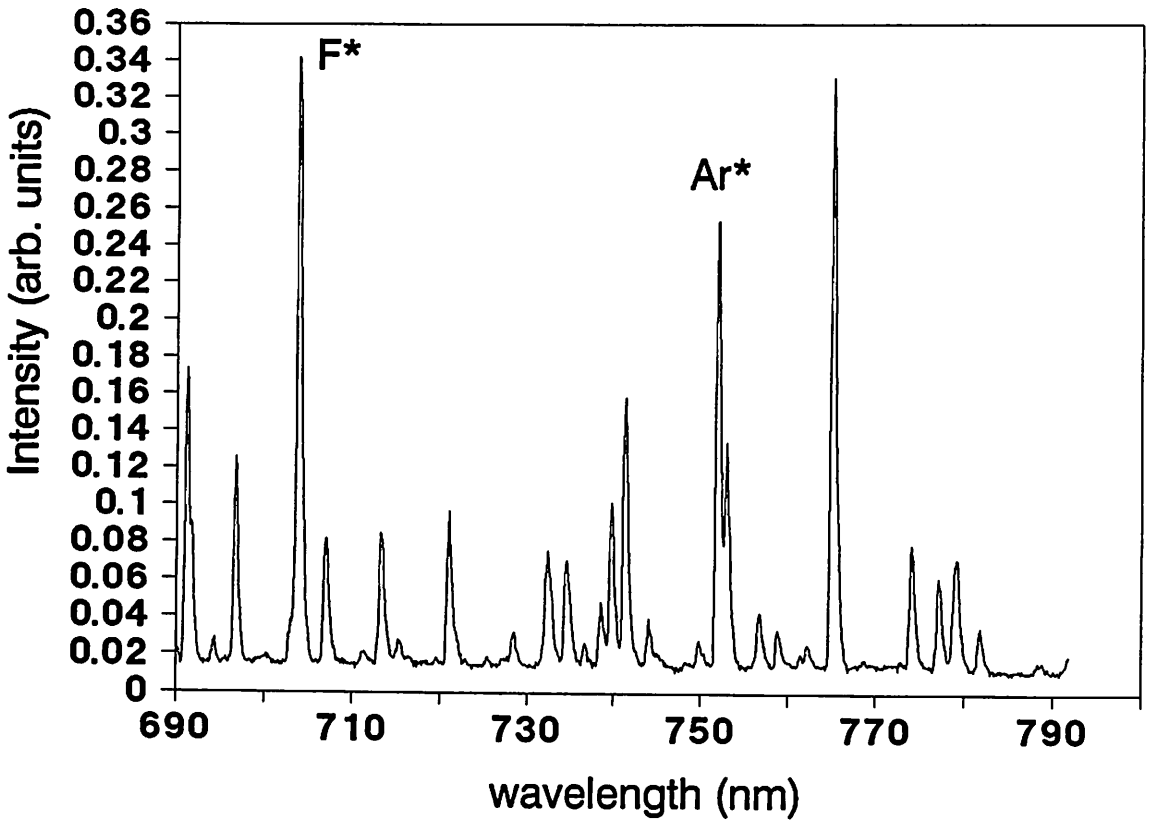

Figure 9. Typical OES spectrum with F* emission line at 703.7 nm and Ar* line at 750.4 nm.

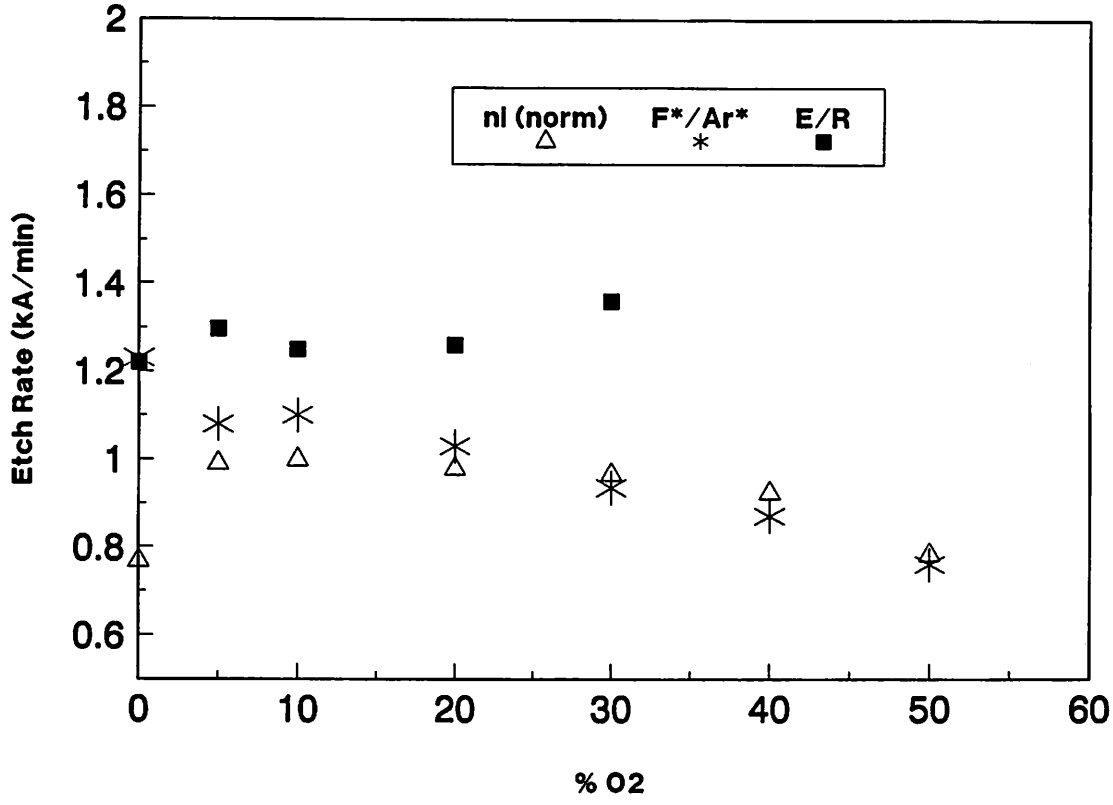

Figure 10. Etch rate, normalized ion density, and relative fluorine atom concentration versus oxygen addition.

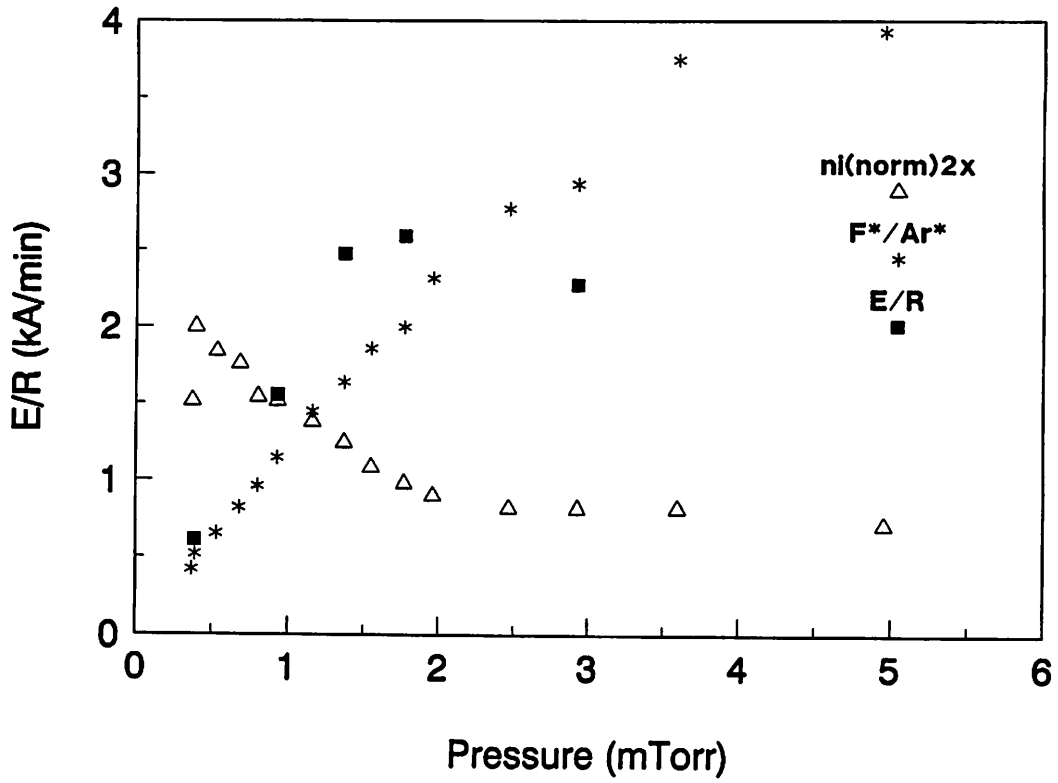

Figure 11. Etch rate, normalized ion density, and relative fluorine atom concentration versus pressure.